



Experimental Vessel for JUPITER

R.R. Peterson, R.L. Engelstad, H.Y. Khater, Y.-M. Lee,
S.C. Rutledge

May 1994

UWFDM-946

FUSION TECHNOLOGY INSTITUTE
UNIVERSITY OF WISCONSIN
MADISON WISCONSIN

DISCLAIMER

This report was prepared as an account of work sponsored by an agency of the United States Government. Neither the United States Government, nor any agency thereof, nor any of their employees, makes any warranty, express or implied, or assumes any legal liability or responsibility for the accuracy, completeness, or usefulness of any information, apparatus, product, or process disclosed, or represents that its use would not infringe privately owned rights. Reference herein to any specific commercial product, process, or service by trade name, trademark, manufacturer, or otherwise, does not necessarily constitute or imply its endorsement, recommendation, or favoring by the United States Government or any agency thereof. The views and opinions of authors expressed herein do not necessarily state or reflect those of the United States Government or any agency thereof.

Experimental Vessel for JUPITER

R. R. Peterson, R. L. Engelstad, H. Y. Khater,
Y.-M. Lee and S. C. Rutledge

Fusion Technology Institute
University of Wisconsin-Madison
Madison, WI 53706

May 1994

UWFDM-946

1. Introduction

JUPITER is a concept for a facility to produce large amounts of x rays for simulation of nuclear weapons effects, weapons physics, and other Department of Energy and Department of Defense interests [1]. Primary issues which JUPITER could be used to study are thermomechanical shock, vaporization and blowoff, impulsive pressures, structural response, shock waves and sensor blinding [2]. Secondary issues include Hohlraum physics, radiation flow, opacity, shock physics, mix, and equation-of-state. JUPITER uses some form of pulsed power, flowing down transmission lines into a Plasma Radiation Source (PRS), which produces several MJ of x rays with various spectra up to and above 30 keV. The spectrum and energy required from the PRS is determined by the simulation requirements. The x ray energy varies as the spectrum changes. As of November 1993 [3], it was thought that the required energy was as shown in Table 1. The five photon bins represent different testing requirements and have different required fluences and test area sizes. The required x ray yields for each photon bin are set by the required fluence and the distance that the x-ray irradiated sample must be placed from the PRS. It is assumed that samples require 80% uniformity across a flat surface for bins A, B, and C, and 90% for bins D and E, given the sample size and the assumption that the PRS is a point source of radiation, a minimum uniformity distance is calculated. The x-ray yield that would be required from the PRS to obtain the required fluence, assuming a filter transmission factor of 0.8, and the required uniformity, is called the uniformity yield. The x-ray irradiation must be not only uniform, but must be free enough from the debris damage to the test object that the test faithfully simulates the desired condition. The debris is created in the region of the PRS by a number of means, including the motion of the PRS material, x-ray vaporization of structures close to the PRS and spall and fracture caused by intense magnetic pressures near the PRS. Debris mitigation systems will keep debris fluences on the test object acceptably low. Debris mitigation systems will include filters, shutters and baffles, and will require a distance from the PRS that is determined by considerations like the speed of the debris, shutter apertures and the allowable speed of shuttering materials. This debris mitigation distance is a subject of some controversy and the values used here are consistent with values used by Giuliani [3]. The debris mitigation distances, a fluence loss due to filter transmission and the required fluence leads to the debris mitigation yield. The required yield for each bin is the maximum of the debris mitigation yield and the uniformity yield. In all cases, the debris yield dominates.

Table 1. JUPITER X-Ray Requirements

Photon Bin (keV)	Required Fluence (cal/cm ²)	Test Area (cm ²)	Test Radius (cm)	Uniformity Distance (cm)	Uniformity Yield (kJ)	Debris Mitigation Distance (cm)	Debris Yield (kJ)
A (≤ 1)	1	2.5×10^4	89	178	2093	300	5916
B (1 - 5)	1	2×10^4	80	160	1675	250	4110
C (5 - 15)	1	1×10^4	56	113	837	175	2014
D (15 - 30)	5	60	4.4	13.2	57	50	822
E (30 - 60)	5	25	2.8	8.4	23	30	296

The large x ray yields required for JUPITER to meet its mission make the JUPITER experimental vessel a very harsh environment. The x-ray fluences on the vessel walls will most certainly be high enough to cause some damage. The high yield and high photon energies will require a PRS current that will generate very high magnetic pressures, that can accelerate damaging shrapnel to move throughout the vessel. The mechanical loading on the walls from the shrapnel, the x-ray vaporization and the long term pressure rise in the experimental vessel volume will generate transient stresses which must be designed against. The transmission lines that carry the power to the PRS will be partially destroyed by the very high current density near the PRS and the x-ray vaporization. The transmission line far enough away from the PRS to avoid these effects must be designed to survive the shrapnel and pressure pulses and avoid contamination by blast driven dust. Finally, the transmission lines and PRS will experience voltage drops of 8 to 10 MV, high enough to generate protons that can activate materials. So, some part of JUPITER will be radioactive to some degree, which needs to be quantified and shielded against if necessary.

Initial scoping studies have been performed for the experimental vessel of JUPITER. First, a design is presented for the chamber. The simulations are presented for the vaporization of material from the target chamber walls and from current return posts near the PRS. The mechanical response of the vessel walls to the vaporization of wall material has been considered, and a wall thickness suggested. Finally, some comments are made on radioactivity induced in the facility by Bremsstrahlung and energetic protons.

2. Experimental Chamber Design

The experimental vessel of JUPITER is where the testing requirements meet the realities of what the pulsed power can provide. The chamber must provide an environment in which experiments can be performed in a safe and timely manner. The chamber must also allow for the efficient flow of the pulsed power energy into the PRS, while protecting the accelerator equipment from damaging effects of the blast generated by the PRS. We have arrived at a “strawman” design of the chamber, shown in Fig. 1, which is an attempt to meet the requirements of the users and the pulsed power engineers. The design will change as analysis on and critique of this design proceeds.

There are many trade-offs to be made in the vessel design. As the design of JUPITER proceeds, issues must be balanced against others to obtain an optimum design. Some of trade-offs are listed here:

1. **Lined Wall versus Bare Wall.** A wall that is lined with a material like graphite could reduce the amount of vaporization and a complex liner could reduce the threat to the wall from energetic projectiles. This could lead to thinner and, therefore, lighter and cheaper walls. However, liners could require replacement, adding to costs and maintenance times.
2. **Wall Radius versus Debris Mitigation Distance.** Debris mitigation distances are a function of the debris source and the required irradiation solid angle. It may be possible to have the debris mitigation system extend out beyond the chamber wall, allowing a longer debris mitigation distance than the chamber radius. In some shots, the debris mitigation and the sample will be well within the chamber.
3. **Vessel Height versus Horizontally Mounted Experiments.** The mounting of experiments horizontally will be easier for experimenters. An entire diagnostic system could be moved into position on trailers. This will require the lowering of the PRS to a point below the convolute disk. This will be achieved with a conical power feed. The chamber will have to be high enough to allow the mounting of the experiment, which will have an impact on the vessel cost and weight.
4. **Conical Power Feeds versus Pulsed Power Transmission Losses.** The conical power feeds required for horizontal experimental access will have longer transmission lengths than a planar disk arrangement. This will mean larger losses during transmission and larger transmission inductance. This will lead to more costly pulsed power.

JUPITER VACUUM CHAMBER

UNIVERSITY OF WISCONSIN

12/2/93

Dimensions in cm

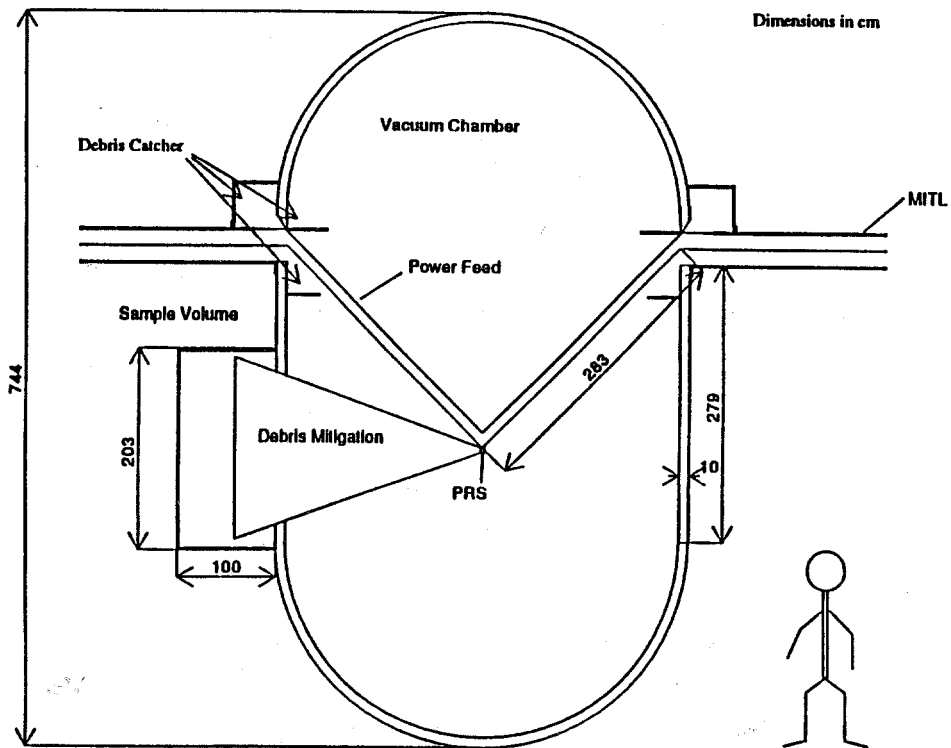


Figure 1. "Strawman" experimental vessel design.

5. **Passive Debris Catcher versus Explosive Valves.** Flow of debris into the convolute and MITL's will be controlled with either passive or active means. Passive debris catchers will use baffles and chambers to direct the debris away from the opening to the convolute. The opening will not be physically closed off. Alternatively, explosive fast closing valves would physically close off the openings, perhaps leading to less debris flow into the convolute. However, explosive valves would lead to a more complicated setup of the experimental vessel for each shot and would destroy the final section of the power feed. The power feed may be destroyed by the intense current density and the blast from the PRS anyway, so the trade-off may come down to a small amount of debris flowing into the convolute versus the complication and safety aspects of explosively driven valves.

3. Vaporization of First Wall and Close-in Material

Computer simulations have been performed to assess the problem of x-ray induced blow-off of material from the vessel walls and from current return pins, that are very close to the PRS. X-ray vaporization from the wall will lead to a vapor load in the vessel that can contribute to the overall debris flow and will generate an impulse on the wall that will induce oscillatory motion. The return current pins will add significant debris through x-ray vaporization and will be accelerated through magnetic forces and the impulse from x-ray blow-off.

The simulations were done with the CONRAD computer code [4]. CONRAD is a one-dimensional Lagrangian hydrodynamics code, with multigroup radiation diffusion. Time-dependent x-ray and debris ion sources are included. Vaporization, including the effects of x-rays, ions, energy radiated from the already vaporized material, and thermal condition in the unvaporized material, is calculated by CONRAD. The high density equations-of-state of the material, except for the contribution from atomic excitations, is calculated from a Mie-Grueneissen model that includes the effects of degenerate electrons and relaxes to the standard solid-state based on the bulk properties of the material at solid density. At gas densities, the model relaxes to a γ law gas. The atomic excitation part of the equations-of-state and opacities are read from tables generated by the IONMIX [5] computer code. This model is similar to the ANEOS method [6], and it agrees with the SESAME [7] data over a wide range. The x-ray deposition is calculated with cold stopping powers that are determined from analytic fits to experimental data [8], and where the stopping power is reduced by the de-population of the absorbing atomic levels to account for bleaching.

Table 2. Parameters for CONRAD Simulations of X-Ray Blow-Off

	Return Current Pins	First Wall
Material	Steel	Steel
Bin A energy (MJ)	3.5	3.5
Bin B energy (MJ)	4.8	4.8
Distance from PRS (cm)	6.3	200
Bin A pulse width (ns)	100	100
Bin B pulse width (ns)	20	20
Bin A pulse start (ns)	0	0
Bin B pulse start (ns)	40	40
Bin A fluence (J/cm ²)	6960	6.96
Bin B fluence (J/cm ²)	9600	9.60
Total x-ray fluence (J/cm ²)	16560	16.56

Simulations are performed for the parameters in Table 2. The x-ray source consists of a broad (100 ns) pulse of 100 eV blackbody spectrum photons (Bin A) and short (20 ns) argon K line (Bin B) x rays centered on the Bin A pulse. The time dependent x-ray spectrum is shown in Fig. 2. We believe that these conditions will be about the worst one could expect, from the point of view of x-ray vaporization. The higher photon energy bins have lower fluences and longer penetration lengths in the material, leading to lower specific power deposition, and therefore lower shock pressures and less material vaporization.

The results of these CONRAD simulations are summarized in Table 3 and in Figs. 3 and 4. The simulation for the current return pins (Fig. 3) show a massive amount of vaporization (20 μm , 15 mg/cm²), leading to a huge pressure and impulse on the pins. Vaporization of the pins is due to both Bin A and Bin B x rays. Vaporization of the first wall (Fig. 4) is much lower (0.9 μm , 0.7 mg/cm²). The resulting impulsive pressure on the wall is 20 Pa-s. In this case, vaporization is mostly due to Bin B photons.

The current return pins experience both x-ray blowoff and magnetic forces. We can estimate the magnetic forces by considering the forces between all of the pins, each carrying an equal parallel current, I , and between each pin and an anti-parallel current of $N \times I$ in the center of the PRS, where N is the number of pins. We assume that there are 8 pins equally spaced on a circle, 6.3 cm in radius. The force per unit length of wire,

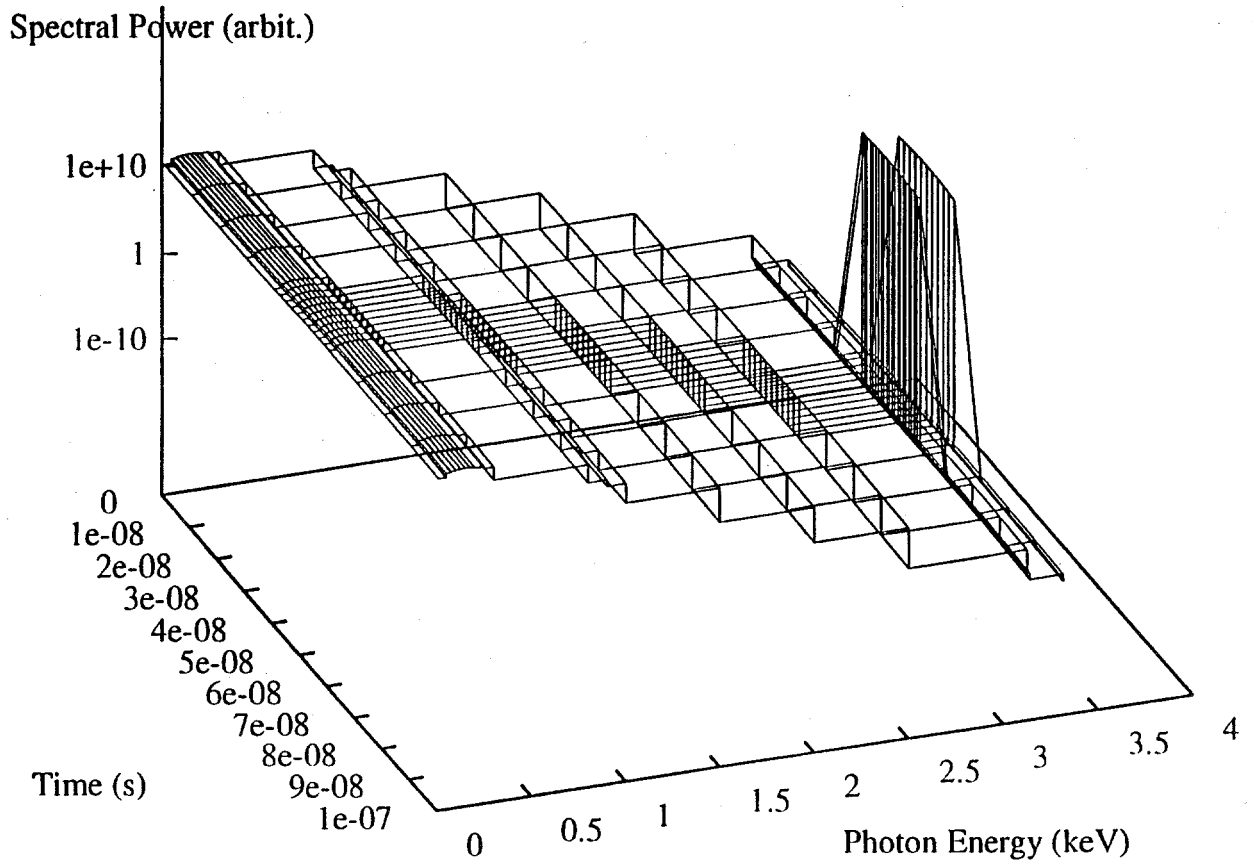


Figure 2. Assumed time-dependent JUPITER x-ray spectrum.

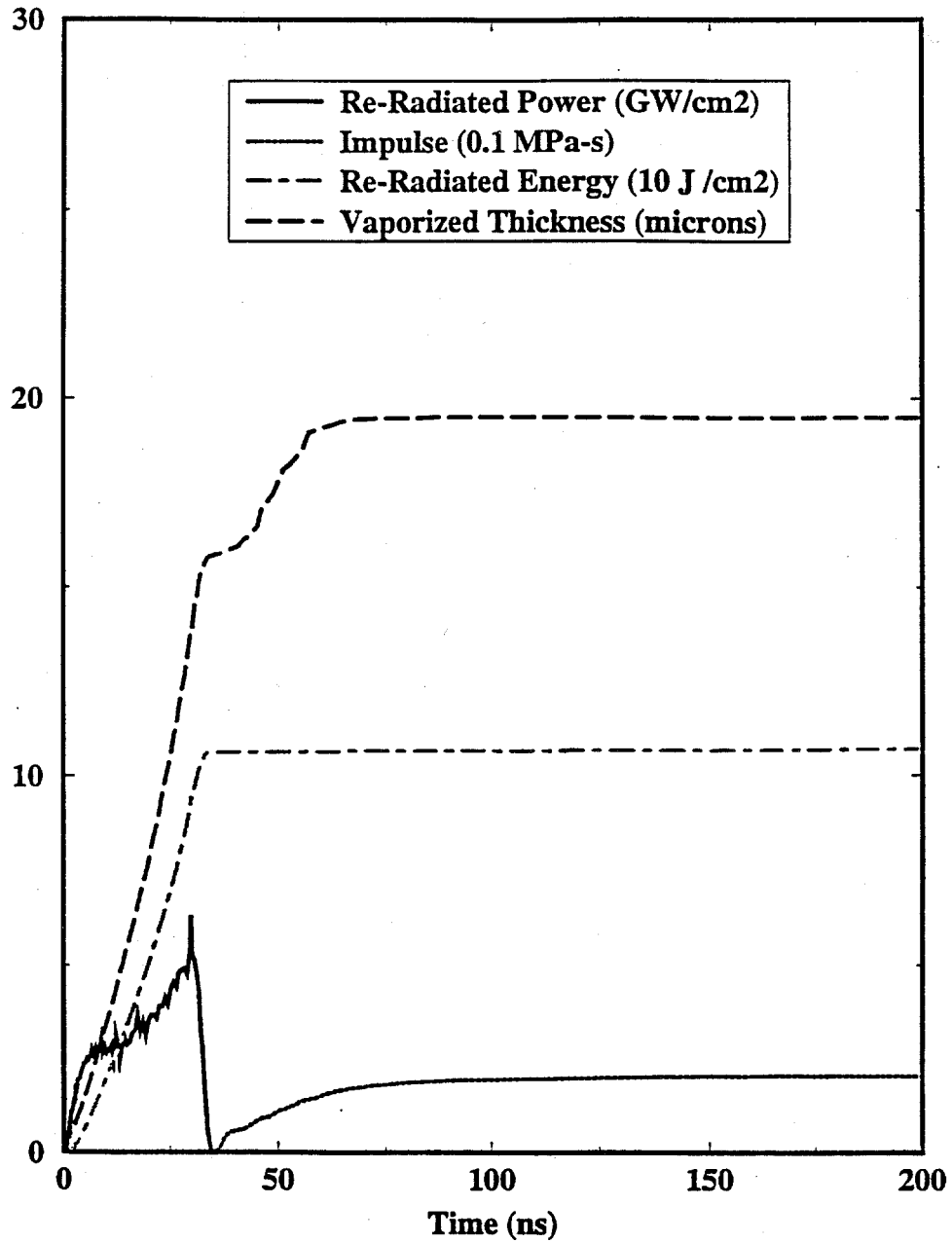


Figure 3. Results of CONRAD simulations for x-ray vaporization from current return pins. Vaporized thickness, power re-radiated from the vapor to the unvaporized surface, integrated energy re-radiated from the vapor to the surface and the resulting mechanical impulse on the surface are shown versus time.

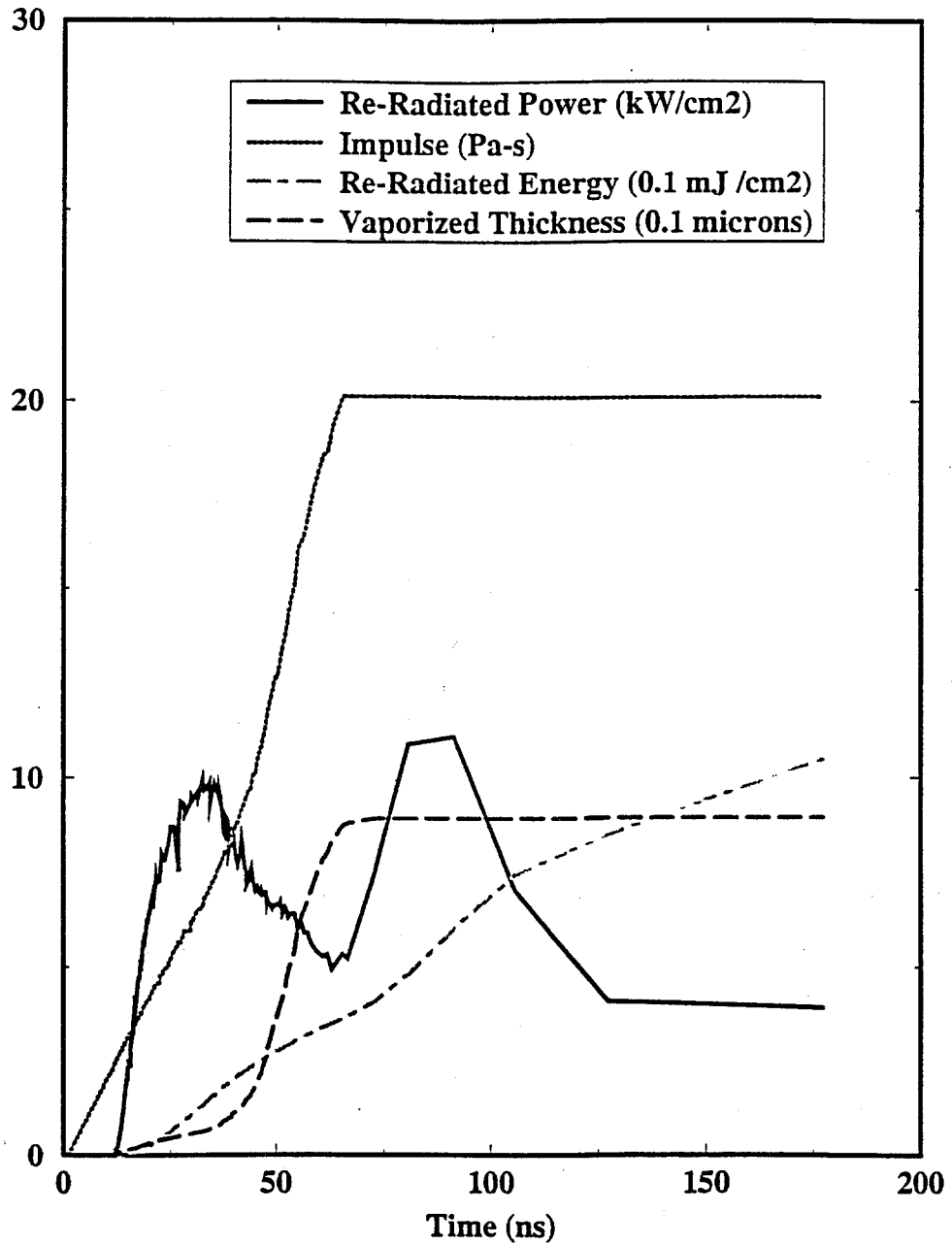


Figure 4. Results of CONRAD simulations for x-ray vaporization from vessel first wall. Vaporized thickness, power re-radiated from the vapor to the unvaporized surface, integrated energy re-radiated from the vapor to the surface and the resulting mechanical impulse on the surface are shown versus time.

Table 3. Results of CONRAD Simulations of X-Ray Blow-Off

	Return Current Pins	First Wall
Mass vaporized (mg/cm ²)	15.4	0.71
Vaporized thickness (μm)	19.5	0.90
Energy re-radiated to surface (J/cm ²)	107	1.05×10^{-3}
Peak re-radiated power (W/cm ²)	6.30×10^9	1.17×10^4
Peak pressure on surface (GPa)	2.53×10^4	22.1
Impulsive pressure (Pa-s)	2.06×10^5	20.1

in dynes/cm, between two wires, d cm apart, carrying currents I_1 and I_2 in amps is,

$$\vec{F} = \frac{I_1 I_2}{5d}. \quad (1)$$

The azimuthal component of \vec{F} about the circle of pins will vanish, as will the component parallel to the current if we neglect end effects. Summing the radial components of \vec{F} on a pin from the seven other pins and the return current down the center of the PRS,

$$F_r = \frac{.9I^2}{r}, \quad (2)$$

where r is the radius of the circle. For a total current of 60 MA, I is 7.5 MA and F_r is 8.04×10^{12} dynes/cm. If we assume a 100 ns flat top current pulse, the magnetic impulse per unit length on each pin is 8.04×10^5 dyne-s/cm. The x-ray blowoff impulsive pressure, the impulse per unit area, is 2.06×10^5 Pa-s, or 2.06×10^6 dyne-s/cm². If the pins are 0.5 cm in diameter, the x-ray force per unit length is 1.03×10^6 dyne-s/cm. Therefore, within the levels of approximation taken herein, the x-ray blow-off and magnetic forces on the pins are equal, and the total impulse per unit length is 1.83×10^6 dyne-s/cm. If the pins are made of steel, the mass per unit length is 1.6 g/cm. If the momentum lost in shearing-off and deforming the pin is ignored, the maximum velocity of the pin is 1.1×10^6 cm/s. The velocity of spalled or melted material could be greater.

The vapor load from the x-ray vaporization of these pins, if they are assumed to be 5 cm long, is 0.31 g of steel. The wall adds about 400 g of steel vapor to the system. Its flow throughout the vessel has not been analyzed.

4. Mechanical Response of the First Wall

The JUPITER target chamber was modeled as a thin-walled cylindrical shell with rigidly clamped end conditions that are allowed to expand axially. The general equations of motion for the dynamic response of the cylinder [9] were then used to calculate displacement and stress histories at critical locations. Both membrane stresses and bending stresses were included in the structural analysis, but the effect of wall perforations was neglected. With the rigid end conditions, the maximum normal stress would occur near the supports. However, it was assumed that the thickness of the cylinder would be increased in this location to control localized stresses. Consequently, the maximum stress will be a circumferential normal stress at the midspan of the cylinder. The longitudinal stress at this location would be zero.

The external loading consisted of two components. The first was an initial impulsive pressure corresponding to the 20 Pa-s previously computed by the CONRAD code. The second was a residual after-pressure (approximately 0.5 MPa) present in the cylinder due to the energy that remains in the debris for a relatively “long” period of time, resulting in a “step” loading of the cylinder. These pressure loads were assumed to be uniformly distributed over the chamber wall, which produced an axisymmetric response of the cylinder.

Numerical calculations were then performed to determine the dynamic response of the first wall as a function of time. A damping coefficient of 2% was used in all computations and 20 modes were summed in the solution of the equations of motion [9]. Figure 5 shows the maximum stress (at the midspan) as a function of time for a wall thickness of 5 cm. Note that the dynamic stresses are damping out to a steady state stress consistent with the residual overpressure. Parametric calculations were performed to generate design curves for determining the appropriate thickness. Fig. 6 shows the maximum value of the dynamic stress as a function of thickness. A thickness of 2.5 cm appears to be a reasonable value, allowing for factors of safety, etc. It should be noted that a fatigue analysis has not been performed as part of this study, but would be recommended for future analyses.

5. Radioactivity

The radioactivity induced in the facility has been very crudely estimated. Activation by 8, 10, and 12 MeV Bremsstrahlung and 8, 10 and 12 MeV protons in ^9Be , ^{27}Al , and ^{56}Fe through (γ, n) and (p, n) transmutations occurs. Since all three materials

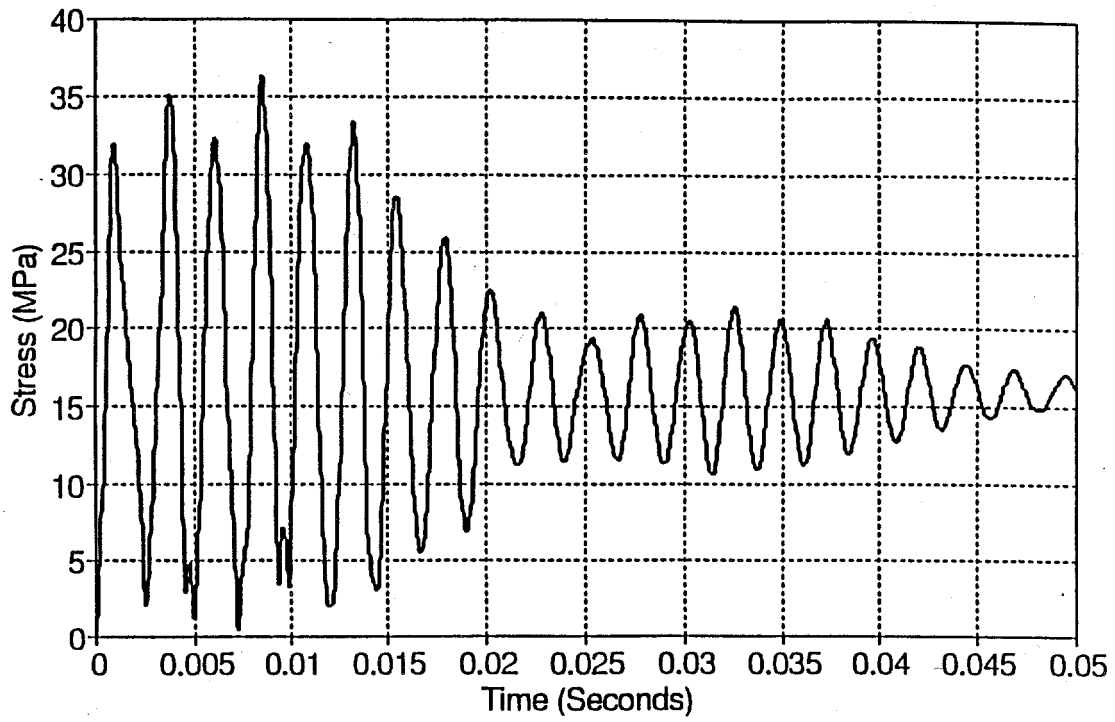


Figure 5. Time-dependent stresses in a 5 cm thick steel vessel wall. The wall is loaded with a 20.1 Pa-s impulsive pressure and a 0.5 Pa steady state pressure due to energy contained in the vessel debris.

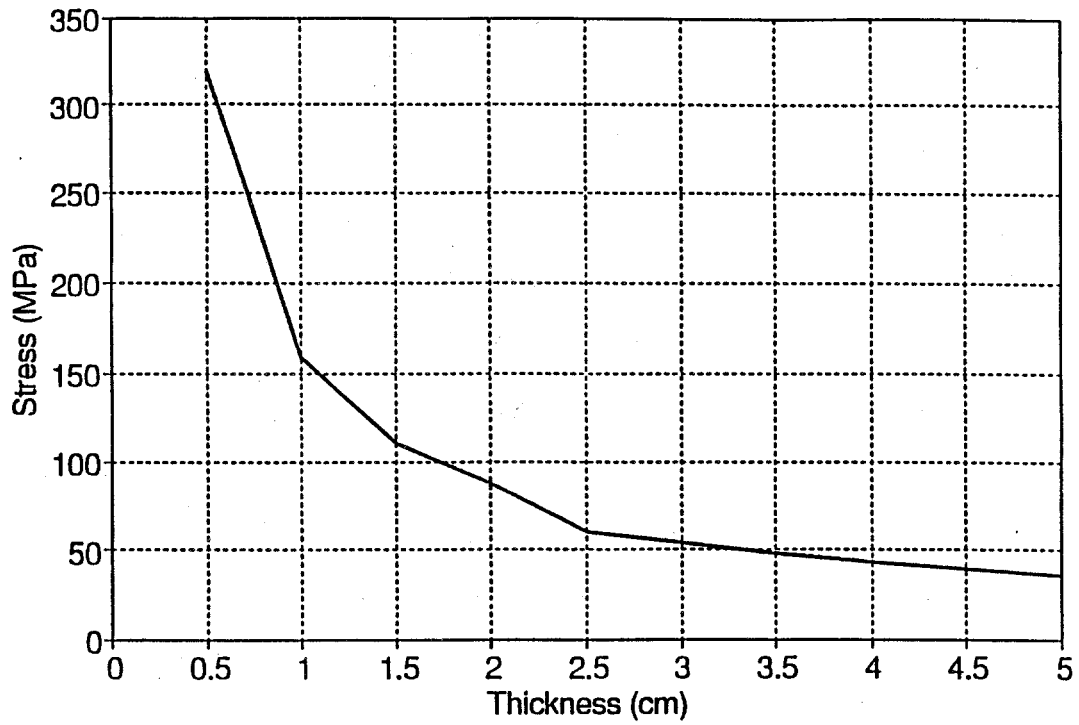


Figure 6. Peak wall stress versus wall thickness. The wall is loaded with a 20.1 Pa-s impulsive pressure and a 0.5 Pa steady state pressure due to energy contained in the vessel debris.

examined have small (γ, n) cross sections at or below a γ energy of 12 MeV, the resulting induced activity is expected to be very small. On the other hand, the (p,n) cross sections are more significant, and hence a preliminary analysis to examine the impact of proton activation is performed.

The main difficulty in the analysis of activation by protons is the need to use nuclear cross sections. The nuclear cross section is not a convenient quantity to use for this purpose because it is strongly dependent on the proton energy, such that it continually varies as the protons slow down in the irradiated material. One alternative quantity to the cross section that is widely used is the thick-target yield “Y”, which is usually expressed in the units of $\mu\text{Ci}/\mu\text{A}\cdot\text{hr}$.

An equation that describes the thick-target yield of a radioactive isotope produced from a stable nuclide can be written as:

$$Y = 1.69 \times 10^8 n \lambda \int_0^{E_p} \frac{\sigma(E)}{S(E)} dE, \quad (3)$$

where n is the parent (stable) atom concentration in atoms/g, λ is the radioisotope decay constant in hr^{-1} , E_p is the proton energy in MeV, $\sigma(E)$ is the parent atom (p,n) cross section in cm^2 , and $S(E)$ is the parent atom stopping power in $\text{MeV}\cdot\text{cm}^2/\text{g}$.

While experimental cross section data were collected from several publications [10, 11], the proton stopping powers were taken from the most complete data sets compiled by Anderson and Ziegler [12].

From the definition of the thick-target yield “Y” of any radioactive isotope, the activity produced takes the form:

$$A = YI \left(\frac{1 - e^{-\lambda t}}{\lambda} \right) \quad (4)$$

where I is the proton current in μA and t is the irradiation time in hours.

If a radioactive isotope “i” is produced as the result of a proton interacting with its parent nuclide “j”, which is in turn contained as a homogeneous admixture to the irradiated structural material “k”, the activity produced is:

$$A_{jk}^i = Y_{jk} I (1 - e^{-\lambda_i t}) \quad (5)$$

where,

$$Y_{jk} = Y \eta_{jk} F. \quad (6)$$

Here, Y is the thick-target yield of the radioisotope “i” for a thick target consisting entirely of its parent nuclide “j”, η_{jk} is the relative concentration (by weight) of the

nuclide “j” in the target “k” and λ_i is the radioactive decay constant of isotope “i”. F is a factor, which takes into account the difference between the proton stopping power of the parent nuclide “j” and that of the irradiated alloy “k”. F can be defined as:

$$F = \frac{R_k}{R_j} = \frac{1}{x_1 + x_2 \frac{R_1}{R_2} + x_3 \frac{R_1}{R_3} + \dots} \quad (7)$$

Here, R_j is the range of protons in the parent nuclide “j”, R_k is the range of protons in the irradiated alloy “k” and R_1, R_2, R_3, \dots are the ranges of protons in the individual nuclides forming the irradiated alloy “k”. x_1, x_2, x_3, \dots are the weight proportions of the individual elements in the target compound.

If the radioisotope “i” is formed simultaneously from several stable nuclides in the target, then the radioisotope activity can be written as:

$$A_k^i = I(1 - e^{-\lambda_i t}) \sum_n Y_{nk} \quad (8)$$

The index “n” refers to a parent nuclide in the target that produces the radioactive nuclide from interaction with the incident proton.

${}^9\text{B}$, with a half-life of 8×10^{-19} s, and ${}^{27}\text{Si}$, with a half-life of 4.14 s, are produced by proton interactions with ${}^9\text{Be}$ and ${}^{27}\text{Al}$, respectively. Since both radionuclides have short half-lives, they should have little effect on the operation of JUPITER. The only (p,n) reaction that could produce significant long-term activation is with Fe. Protons interacting with ${}^{56}\text{Fe}$ will produce ${}^{56}\text{Co}$, which has a 77.3 day half-life. If JUPITER is fired at a rate of 2 shots a day for a year, with all of the current going into protons stopped in Fe, the 8, 10 and 12 MeV protons will lead to the production of 0.05, 0.61 and 5.1 Ci respectively.

This is a preliminary calculation, which can be misleading because other constituents and impurities of the beryllium, aluminum and steel alloys could dominate the level of induced activity. This effect needs to be considered once the facility design has progressed to the point where the materials, geometry and proton fluences and spectra are better known. At that point the radioactivity can be calculated throughout the facility and shields can be designed.

6. Conclusion

The JUPITER experimental chamber has been studied in a preliminary way. In order to identify issues of concern in the design of the JUPITER experimental chamber a “strawman” design has been presented and analyzed. The general results of this exercise are as follows:

1. Significant material is vaporized from the current return pins by the PRS x rays. Very large impulsive pressures are applied to the pins by the x rays (2.06×10^5 Pa-s). If the pins are 0.5 cm in diameter, the magnetic forces apply roughly an equal impulse per unit area. The maximum possible velocity of the whole pin is 1.1×10^6 cm/s. If the 8 pins are 5 cm long, 0.31 g of steel vapor is added to the debris source.
2. X rays also vaporize some material from the experimental vessel walls. Approximately 400 g of steel are vaporized from the walls. The resulting impulsive pressure on the walls is 20 Pa-s. This and the assumed long term pressure in the vessel from the vapor of 0.5 MPa results in vibration of the wall that dictates that the wall should be at least 2.5 cm thick, leading to a vessel that weighs 17 metric tons.
3. Activation by 8 to 12 MeV protons and Bremsstrahlung has been estimated in Al, Be and Fe. Preliminary calculations show that Bremsstrahlung induced activation is not a concern for these materials because the photon energies fall below the (γ, n) thresholds. Activation by protons does occur, but the preliminary estimates lead to a low level of radioactivity, the worst material being Fe.

Once more details of the pulsed power, the PRS, the debris mitigation and the experimental requirements are known, all of these items should be revisited. Some things that should be done are:

1. Recalculate the debris source terms due to x rays and magnetic fields in the PRS region.
2. Redesign an experimental vessel, integrating with the pulsed power, debris mitigation, and experiments. Use refined PRS results for the x-ray and debris loads and consider the full range of possible PRS performance. Consider the flow of debris in the vessel and design a system to control the flow into the power feeds.

3. Reconsider the activation issues using the full geometry and materials list of the complete design and then design a shield system to protect personnel and equipment from both pulsed and long term sources. Consider decommissioning and waste disposal.

Acknowledgement

Support for this work has been provided by Sandia National Laboratories.

References

- [1] J. R. Lee, et al., “Justification of Mission Need for the Jupiter Project,” Appendix 1, JDOST Interim Report (30 December 1993).
- [2] W. Beezhold, “Summary of DOE Mission Needs,” JDOST-3, Sandia National Laboratories, October 26, 1993.
- [3] J. L. Guiliani, Jr., “Test Requirements/Capabilities Matrix for the JUPITER Simulator,” un-numbered memorandum, Naval Research Laboratory (November 16, 1993).
- [4] R. R. Peterson, J. J. MacFarlane, and G. A. Moses, “CONRAD – A Combined Hydrodynamics–Condensation/Vaporization Computer Code,” University of Wisconsin Fusion Technology Institute Report UWDFM-670 (July 1988).
- [5] J. J. MacFarlane, “IONMIX – A Code for Computing the Equation of State and Radiative Properties of LTE and Non-LTE Plasmas,” *Comp. Phys. Comm.*, **56**, 259 (1989).
- [6] S.L. Thompson and H.S. Lauson, “Improvements in the Chart D Radiation-Hydrodynamics CODE III: Revised Analytic Equations of State,” Sandia National Laboratories Report SC-RR-710714 (March 1972).
- [7] B. I. Bennett, J. D. Johnson, G. I. Kerley, and G. T. Rood, “Recent Developments in the Sesame Equation-of-State Library,” Los Alamos National Laboratories Report LA-7130 (February 1978).
- [8] F. Biggs and R. Lighthill, “Analytical Approximations for X-Ray Cross Sections III,” Sandia National Laboratories Report SAND-0070 (August 1988).
- [9] J. Powers, “Structural and Fatigue Analysis of the Sandia Laboratory Microfusion Reactor Chamber,” University of Wisconsin - Madison, M.S. Thesis, 1991.
- [10] H. Munzel, et al., “Karlsruhe Charged Particle Reaction Data Compilation,” Physics Data, No. 15, Fachinformationszentrum, Karlsruhe (1982).
- [11] National Nuclear Data Center, “On-Line Data Bases,” Brookhaven National Laboratory (1990).
- [12] H. H. Anderson and J. F. Ziegler, “Hydrogen Stopping Powers and Ranges in All Elements,” Pergamon Press, New York (1977).

DISCLAIMER

This report was prepared as an account of work sponsored by an agency of the United States Government. Neither the United States Government, nor any agency thereof, nor any of their employees, makes any warranty, express or implied, or assumes any legal liability or responsibility for the accuracy, completeness, or usefulness of any information, apparatus, product, or process disclosed, or represents that its use would not infringe privately owned rights. Reference herein to any specific commercial product, process, or service by trade name, trademark, manufacturer, or otherwise, does not necessarily constitute or imply its endorsement, recommendation, or favoring by the United States Government or any agency thereof. The views and opinions of authors expressed herein do not necessarily state or reflect those of the United States Government or any agency thereof.

Experimental Vessel for JUPITER

R.R. Peterson, R.L. Engelstad, H.Y. Khater, Y.-M.
Lee, S.C. Rutledge

Fusion Technology Institute
University of Wisconsin
1500 Engineering Drive
Madison, WI 53706

<http://fti.neep.wisc.edu>

May 1994

UWFDM-946